The Depositional Record
The journal of the International Association of Sedimentologists
Open Access

ORIGINAL RESEARCH ARTICLE

Manganese enrichments near a large gas-hydrate and cold-seep field: a record of past redox and sedimentation events

WESLEY C. INGRAM*, STEPHEN R. MEYERS†, ZHIZHANG SHEN†, HUIFANG XU† and CHRISTOPHER S. MARTENS*

*Department of Marine Sciences, University of North Carolina-Chapel Hill, Chapel Hill, NC 27599, USA (E-mail: MatagordaPetroleum@outlook.com)
†Department of Geoscience, University of Wisconsin-Madison, Madison, WI 53706, USA

Keywords
Biogeochemistry, cold seeps, deep-sea sediments, gas hydrates, manganese, redox boundary.

Manuscript received: 22 February 2016; Accepted: 19 July 2016

doi: 10.1002/dep2.18

ABSTRACT

The spatial distribution, mineralogy, and origin of manganese enrichments surrounding a large gas hydrate and cold seep field (Mississippi Canyon 118, Gulf of Mexico) are investigated in this study, to better constrain their biogeochemical context in deep-sea sediments and to assess how gas hydrates may alter such records. Manganese depth profiles from 10 sediment cores, documented using centimetre-scale X-ray fluorescence core scanning, display highly-enriched 1 to 10 cm thick layers. These manganese-rich layers are more numerous, but of lower concentration, in close proximity to the field, and show no consistent relationship with sedimentology (clay vs. carbonate content) or the established chronostratigraphic framework at the site. X-ray diffraction and sequential dissolution procedures indicate that the manganese enrichments are authigenic carbonates, which formed along a palaeo redox boundary during periods of prolonged steady-state conditions. The hypothesis that spatial heterogeneity of this manganese record is linked to the nearby gas hydrate and cold seep field, by influencing redox conditions and/or sedimentation processes, is investigated here. Results are consistent with more frequent interruption of steady-state sedimentation in closer proximity to the salt-tectonic induced bathymetric mound, which contains the active cold seeps and gas hydrate deposits. Thus, spatial mapping of manganese enrichment horizons provides a tool to reconstruct sedimentation surrounding these volatile sea bed features, yielding a measure of past activity of gas hydrates and cold seeps.

INTRODUCTION

Marine gas hydrates have received much attention due in part to the vast amount of carbon contained within these deposits (Kvenvolden, 1988; Dickens, 2001; Milkov, 2004), and their potential linkages to slope destabilization and past climate events (Nisbet, 1990; Paull *et al.*, 1996, 2003; Haq, 1998; Maslin *et al.*, 1998, 2004; Mienert *et al.*, 2005). These aspects have motivated detailed biogeochemical and geophysical investigations of modern gas hydrates (Sassen *et al.*, 2004; Castellini *et al.*, 2006; McGee, 2006; Brunner, 2007; Lapham *et al.*, 2008, 2010; McGee *et al.*, 2009; Macelloni *et al.*, 2012, 2013; Simonetti *et al.*, 2013; Feng *et al.*, 2014; Martens *et al.*, 2016), and the development of palaeoceanographic proxy approaches to assess the stability of hydrates in Earth's past (Dickens *et al.*, 1995; Dickens, 2003). Unique opportunities to understand marine gas hydrates are provided by integrated studies that seek to link modern and palaeo-perspectives, through the investigation of detailed stratigraphic, sedimentological and geochemical records surrounding present-day gas hydrates (Castellini *et al.*, 2006; Brunner, 2007; Ingram *et al.*, 2010, 2013).

Late Quaternary sedimentation and detailed geochemical records are considered in this study, through an analysis of deep-sea cores recovered from the first National Gas Hydrate Seafloor Observatory (McGee, 2006), located on the northern Gulf of Mexico slope within offshore Federal Lease Block Mississippi Canyon 118 (MC118). A special emphasis is placed on the genesis and interpretation of anomalous Mn enrichments ('Mn-layers') that occur at the MC118 site – documented for the first time

in this study. These Mn-rich layers are investigated for their potential to reconstruct sedimentation and biogeochemical changes at the site, including linkages to the gas hydrate field. The Mn enrichments are revealed in exceptional detail through high-resolution elemental analysis (centimetre-scale) using X-ray fluorescence (XRF) scanning techniques (Richter *et al.*, 2006), applied to a network of 10 deep-sea sediment cores across the MC118 site. The Mn-layers are further characterized via chemical dissolution/extraction procedures and X-ray diffraction (XRD) analysis. This suite of analytical approaches allows a detailed assessment of the spatial distribution of the Mn-layers at the MC118 site, determination of their mineral composition, and evaluation of possible linkages to past redox cycling and/or sedimentation processes. Interpretation of the Mn record is aided by a well-established stratigraphic framework, which includes previous chronostratigraphic (Ingram *et al.*, 2010) and sedimentological (Ingram *et al.*, 2013) studies of the same suite of cores.

Based on the analyses outlined above it is postulated that the Mn-layers at MC118 record the duration of steady-state redox conditions, along a palaeo-redox boundary between oxic and post-oxic sediments, and that movement of this boundary is linked to the gas hydrate and cold seep field through its influence on sedimentation. As will be shown, the distribution and concentration of Mn within the discrete Mn-layers is consistent with more frequent interruption of steady-state conditions closer to the field. This observation reveals a potential new method to evaluate past redox/sedimentation conditions across a wide range of time scales, through detailed characterization of solid-phase Mn profiles, by employing XRF scanning to 'map' movement of past redox boundaries. In addition, results presented here indicate that the MC118 field has influenced sea floor morphology and sedimentation, but has not contributed to a catastrophic slope failure during the last 14 000 years, consistent with prior studies (Ingram *et al.*, 2010).

The MC118 site

The offshore MC118 site includes a large sea floor mound with active cold seeps and gas hydrates (Fig. 1), and is the focus of ongoing geophysical and geochemical monitoring (McGee, 2006; Brunner, 2007; Lapham *et al.*, 2008, 2010; McGee *et al.*, 2009; Macelloni *et al.*, 2012, 2013; Simonetti *et al.*, 2013). The field itself is centred at

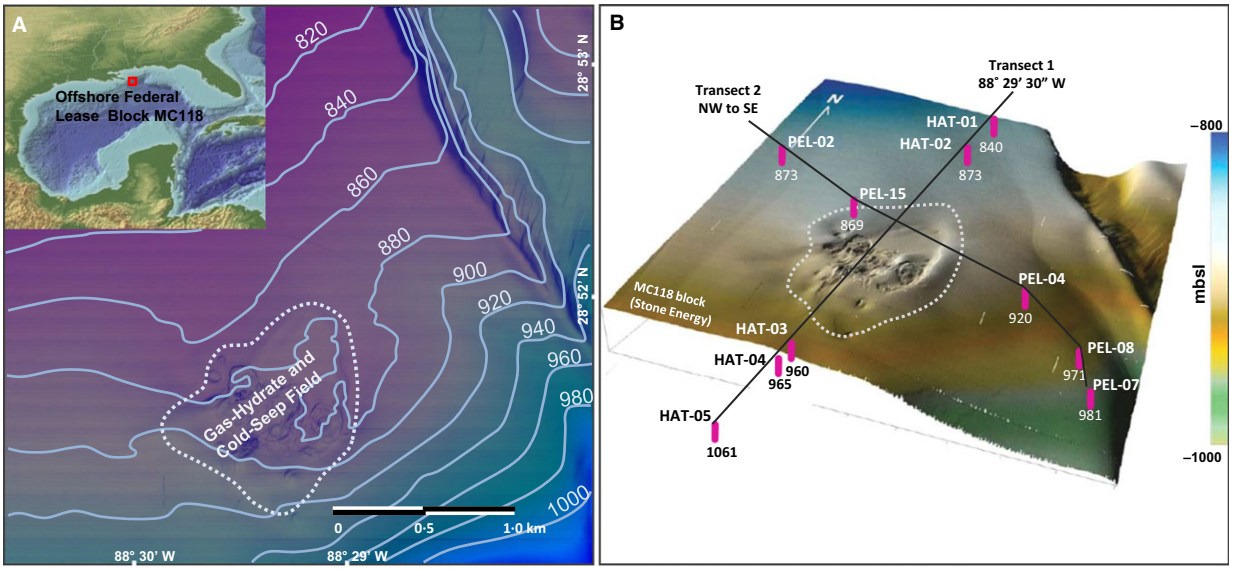

Fig. 1. (A) Bathymetric map of the study area (Block MC118) with labelled contours (light blue) in metres water depth (base map courtesy of Ken Sleeper) with inset digital elevation and bathymetry map (top left; NOAA geophysical data centre image) of the Gulf of Mexico Region. Bathymetry provided by the Gulf of Mexico Hydrate Research Consortium (modified after Sleeper *et al.*, 2006). The location of the MC118 offshore federal lease block is indicated by the red box in the inset map. The extent of the studied gas hydrate-cold seep field is outlined by the dashed line and is characterized by an area with gas vents, sea floor pockmark features, petroleum seepage, shallow faults, carbonate hardgrounds and gas hydrate deposits. (B) Bathymetric map of the study site with the location of cores collected during cruises on the R/V *Hatteras* and R/V *Pelican*; base map image is courtesy of the Gulf of Mexico Hydrate Research Consortium. Cores are indicated as vertical magenta lines, with core identification (above) and water depth (in metres) below the core symbol. The edge of the gas hydrate-cold seep field is outlined by a thin dashed white line, black lines connecting cores indicate transects taken by the R/V *Hatteras* ('Hatteras Transect') and R/V *Pelican* ('Pelican Transect'). The colour bar on the far right indicates water depth (metres below sea level).

28·8523°N and 88·4920°W and lies at approximately 890 m water depth completely within the offshore federal lease block (Fig. 1). Regionally, the northern Gulf of Mexico slope, including this study site, is influenced by salt diapirism beneath the sea floor (Diegel *et al.*, 1995; Jackson, 1995; Galloway *et al.*, 2000). The field is underlain by a salt diapir 200 to 300 m below the sea floor (mbsf), which contributes to the formation of the sea floor mound itself (Sassen *et al.*, 2006; Sleeper *et al.*, 2006). Moreover, the cold-seep mound is the epicentre for the migration and release of hydrocarbons from the sea floor. This supply of hydrocarbons (natural gas and petroleum) supports active biological seep communities (Sassen *et al.*, 2006) and microbial chemolithotrophy in the vicinity of the active seep. The upward migrating hydrocarbons are rapidly cycled and oxidized in shallow sediments, also documented at similar sites in the Gulf of Mexico (Castellini *et al.*, 2006). While intense redox cycling occurs immediately over the MC118 mound, it decreases markedly in sediments outside the field (Lapham *et al.*, 2008). This is important, as the cores used in the present study are positioned mostly outside the area with active seeps, with the exception of Core PEL-15 (Fig. 1). Visible outcroppings of gas hydrates, faulted carbonate 'hardgrounds', authigenic carbonates and pockmark features are present in places across *ca* 1 km^2 of the sea floor in the vicinity of the mound (Sassen *et al.*, 2006; Sleeper *et al.*, 2006; Feng *et al.*, 2014).

Marine gas hydrates are a major feature at this research site, and worldwide they represent a massive reservoir of light hydrocarbons (Milkov, 2004). The vast majority of this carbon occurs in shallow deep-sea sediments along continental slopes (Ginsburg, 1998), such as at MC118. In the Gulf of Mexico, gas hydrates often form alongside cold seeps and supply hydrocarbons to the sea floor, driving substantial changes in both pore-water and sediment chemistry through various redox processes (Sassen *et al.*, 2004, 2006; Paull *et al.*, 2005; Castellini *et al.*, 2006). The present work documents authigenic Mn in deep-sea sediments complicated by nearby gas hydrates and cold seeps, and the cores investigated in this study reflect ambient sea floor conditions as well as those influenced by the mound (Fig. 1).

MATERIAL AND METHODS

Core collection and processing

A total of 10 gravity cores were collected from surface ships, five onboard the R/V *Hatteras* in August, 2007 and five by the R/V *Pelican* in April, 2008 (Sleeper & Lutken, 2008; Ingram *et al.*, 2010; Fig. 1). Cores were transported to and processed at a shore-based laboratory at the University of North Carolina, Chapel Hill, where they were prepared for geochemical analyses (see Ingram *et al.*, 2010, for detailed description of coring and processing methods).

X-ray fluorescence (XRF) core scanning

Cores were analysed using an Avaatech-XRF scanner (2nd generation) with a rhodium target X-ray source, and a Canberra X-PIPS detector. Continuous down-core XRF scanning was conducted at a resolution of 1 cm along the archive-half split core surface (Richter *et al.*, 2006; Ingram *et al.*, 2010). Manganese was scanned using a 10 kV acceleration voltage, 1000 mA, with a cellulose filter, and 90 sec measurement time, with duplicate scans every 10 cm, which yielded highly reproducible results (Table 1). The XRF scanning 'count' data are calibrated (least-squares linear fits; Table 1) to Mn concentration data for selected cores (HAT-03, PEL-04, PEL-07; 54 samples), using Inductively Coupled Plasma Atomic Emission Spectrometry (ICP-AES; SGS Laboratory method ICP-AES 40B, see Table 1 for error analysis).

Reductive and acidification dissolutions

Five Mn-rich layers were sampled from Core PEL-07 to operationally determine the mineral phases associated with the Mn enrichment. Sediment from each depth interval (Mn-layer) was first pulverized into 100-mesh powder. The procedure from Chun *et al.* (2010) was then

Table 1. XRF-ICP Mn Calibration Data: Calibration equations (least-squares linear fits) relating concentration from ICP-AES method to counts from X-ray fluorescence method, Pearson correlation coefficients (r^2 value) and number of samples used for calibration. Average coefficient of variation (CV) ratios for Mn XRF counts (XRF CV) are based on duplicate scans analysed every *ca* 10 cm, and select duplicates from ICP-ES sent to SGS Labs (SGS Laboratory method ICP-AES 40B). Average errors (CV) for XRF counts of Mn are slightly higher than other elements previously measured (Ingram *et al.*, 2010), likely a result of lower concentration of Mn in these marine sediments.

Core	Element	Calibration Eqn.	r^2 Value	Samples
XRF-ICP manganese calibration data				
HAT-03	Mn	$y = 8{\cdot}31*10^{-2}(x) - 55{\cdot}268$	0·84	13
PEL-04	Mn	$y = 4{\cdot}5*10^{-2}(x) + 261{\cdot}57$	0·79	32
PEL-07	Mn	$y = 7{\cdot}25*10^{-2}(x) + 28{\cdot}554$	0·85	9

Core	XRF CV	ICP-ES CV	Core	XRF CV
Average coefficient of variation for Mn				
HAT-01	0·098	NA	PEL-02	0·116
HAT-02	0·137	NA	PEL-15	0·129
HAT-03	0·035	0·008	PEL-04	0·066
HAT-04	0·12	NA	PEL-08	0·106

used to remove oxides and oxyhydroxides by reductive dissolution, followed by an acid dissolution step (sodium acetate, pH = 3·96) to remove carbonates, with the remaining residue comprising 'insoluble' clays and/or fine-grained silicates. Manganese and Ti concentrations were measured after each step, using ICP-AES (SGS Laboratory method ICP-AES 40B) on the same split sample from each fraction of the procedure, allowing estimation of: (1) untreated (total Mn), (2) Mn oxide, (3) Mn carbonate, and (4) insoluble residue, which represents the unreactive aluminosilicates (clay content) and/or silicates (Schenau *et al.*, 2002; Chun *et al.*, 2010).

Manganese enrichment factors (EF), EF = $(\text{metal/Ti})_{\text{sample}}/(\text{metal/Ti})_{\text{crust}}$ were calculated to normalize Mn to Ti, a conservative detrital input. 'Excess' Mn (authigenic) was calculated using the following equation [Mn excess = $\text{Mn}_{\text{total}} - (\text{Ti}_{\text{sample}}*(\text{Mn/Ti})_{\text{crust}})$] from Chun *et al.* (2010), and the bulk crustal Mn/Ti ratio (mol/mol) of 0·156 from Rudnick & Gao (2003). Enrichment factors and excess Mn calculations are a means to correct for inadvertent loss of mass during the sequential extraction procedures. These values are used to better constrain the fraction of Mn contained in carbonates versus oxides (Table 2).

X-ray diffraction (XRD) for select Mn-layers

A total of five Mn-layers from Core PEL-07 were analysed by X-ray diffraction. Powder samples were analysed using a Rigaku Rapid II X-ray diffractometre with a 2D detector and Molybdenum Kα radiation operated at 50 kV, 50 mA. Samples were ground to a fine powder and then mounted within capillary glass tubes, which yields improved XRD spectra with lower background compared to standard mounts.

RESULTS

Stratigraphy and XRF scanning results

Ten shallow gravity cores collected around the MC118 field comprise 38·6 m of total recovered sediment (Fig. 2), and reveal a detailed Mn record documented by centimetre-scale XRF core scans. The occurrence of Mn-layers is described in the context of the previously established chronostratigraphy at the site. Detailed sedimentological, stratigraphic and chronostratigraphic information can be found in Ingram *et al.* (2010, 2013) (For the chronostratigraphic framework, see figs 3–6 in Ingram

Table 2. Mn concentrations from ICP-AES determined for sediment samples from authigenic Mn-layers within Core PEL-07. Sediment samples were selected from 5 depths, and subjected to a two-step chemical dissolution to first remove oxide/oxyhydroxides, and then carbonates (see Material and Methods). Mn enrichment factor (Mn-EF) and 'excess' Mn (E. Mn) is also determined for each layer (see Methods; Chun *et al.*, 2010), and is not applicable (NA) for insoluble clay, as 'excess' Mn is defined as the amount which exceeds the siliciclastic fraction, predominantly clay here. The insoluble (clay) fraction is the remaining material after dissolutions and is fine-grained, consisting of clay with minor silts possible. The sample was measured for Mn concentration following each step, and for untreated samples. The Mn concentrations for oxides, carbonates and insoluble (clay), are inferred using the following scheme: oxides = untreated – step 1; carbonates = step 1 – step 2; insoluble (clay) = step 2. The percentage of the total (far right column) is a ratio of Mn in each fraction, oxides, carbonates and insoluble (clay), relative to the untreated sample or total Mn.

Core	Depth	Dissolution	Mn (p.p.m.)	Ti (p.p.m.)	Mn EF	E. Mn (p.p.m.)	Composition	Mn (p.p.m.)	% Total (from p.p.m.)
Mn species data to solve for Mn mineral									
PEL-07	130	Untreated	2800	2900	5·393	2347	Oxyhydroxides	160	5·71
PEL-07	130	Step 1	2640	3100	4·756	2156	Carbonates	2373	84·75
PEL-07	130	Step 2	267	3600	0·414	NA	Insoluble (Clay)	267	9·54
PEL-07	189	Untreated	1990	2800	3·969	1553	Oxyhydroxides	60	3·02
PEL-07	189	Step 1	1930	3100	3·477	1446	Carbonates	1674	84·12
PEL-07	189	Step 2	256	3300	0·433	NA	Insoluble (Clay)	256	12·86
PEL-07	212	Untreated	1670	2800	3·331	1233	Oxyhydroxides	90	5·39
PEL-07	212	Step 1	1580	2900	3·043	1128	Carbonates	1331	79·7
PEL-07	212	Step 2	249	2900	0·48	NA	Insoluble (Clay)	249	14·91
PEL-07	577	Untreated	1610	2700	3·33	1189	Oxyhydroxides	0	0
PEL-07	577	Step 1	1610	2800	3·212	1173	Carbonates	1239	76·96
PEL-07	577	Step 2	371	3200	0·648	NA	Insoluble (Clay)	371	23·04
PEL-07	599	Untreated	2350	2700	4·861	1929	Oxyhydroxides	180	7·66
PEL-07	599	Step 1	2170	2700	4·489	1749	Carbonates	1753	74·6
PEL-07	599	Step 2	417	2700	0·863	NA	Insoluble (Clay)	417	17·74
PEL-07	Avg.	Untreated	2084	2800	4·187	1647	Oxyhydroxides	98	4·36
PEL-07	Avg.	Step 1	1986	2900	3·799	1534	Carbonates	1674	80·02
PEL-07	Avg.	Step 2	312	3100	0·555	NA	Insoluble (Clay)	312	15·62

et al., 2010). Additionally, the previously established stratigraphy is also provided here for visual context of the sedimentological units (Fig. 2).

Shallow sediments of Unit I are informally broken into Units IA and IB to better describe the occurrence of Mn-layers within the larger stratigraphic Unit I (Fig. 2). Sediments of Unit IA are late Holocene in age (*ca* 2300 calendar years BP to present) calcareous nannofossil silty clays, and are laterally discontinuous across the study area. Sediments of underlying Unit IB are also calcareous nannofossil silty clays, but are more nannofossil-rich than the overlying Unit IA. Across all studied cores, the more calcareous Unit IB is generally thicker than Unit IA (Fig. 2), and accumulated over a longer time period (*ca* 2300 to 9500 calendar years BP). Sediments of Unit IB are also lighter in colour and exhibit fewer sedimentary structures (Ingram *et al.*, 2010).

With these sedimentological units defined, the occurrence of Mn-layers is presented in stratigraphic context (Figs 2 and 3). The shallowest Unit IA exhibits very few Mn-layers, with some exceptions. Core HAT-04 displays a shallow Mn-layer completely within Unit IA, and to a lesser extent PEL-04 shows an increased Mn concentration at the top of the core (Fig. 3). With the exception of core HAT-04, all other recovered cores lack discernable Mn-layers within this shallowest stratigraphic interval. Unit IB below also contains few authigenic Mn-layers, with one notable exception, Core HAT-03, which displays two nearly synchronous layers at the base of the unit with Mn content well above 'background' levels (Fig. 3).

Unit II beneath the shallower carbonate-rich interval (Fig. 2) is a mottled, hemipelagic nannofossil silty clay (Ingram *et al.*, 2010). Sediments here are markedly more clay rich with substantially lower carbonate content. This unit appears visually darker with sedimentary structures that are disturbed by burrows in places. Sediments are early Holocene to late Pleistocene in age ranging from 9500 to 14 000 calendar years from the top to the base of the unit (Fig. 2). This interval contains more Mn-layers than any other unit (at least 15 identified layers) with highly pronounced layers in Cores HAT-01, -05 and PEL-02 (Fig. 3). XRF scans of these same three cores also display less numerous Mn-layers, and in places exhibit only one or two, while cores that contain many layers generally yield lower concentrations for the individual layers. Calibration of XRF data indicates these 'more numerous' layers are *ca* 1000 p.p.m. Mn less concentrated than the single or double highly discrete layers (Fig. 3).

A continuation of clay-rich sediments comprises Unit III, a well-laminated hemipelagic nannofossil silty clay, which is differentiated from overlying sediments by numerous red-brown layers (Fig. 2). Sediments of this lowermost unit are chemically and lithologically similar to the unit above, yet with slightly higher lithogenic inputs (Ingram *et al.*, 2013). The top of this unit is marked by a prominent red-brown band ('red band'),

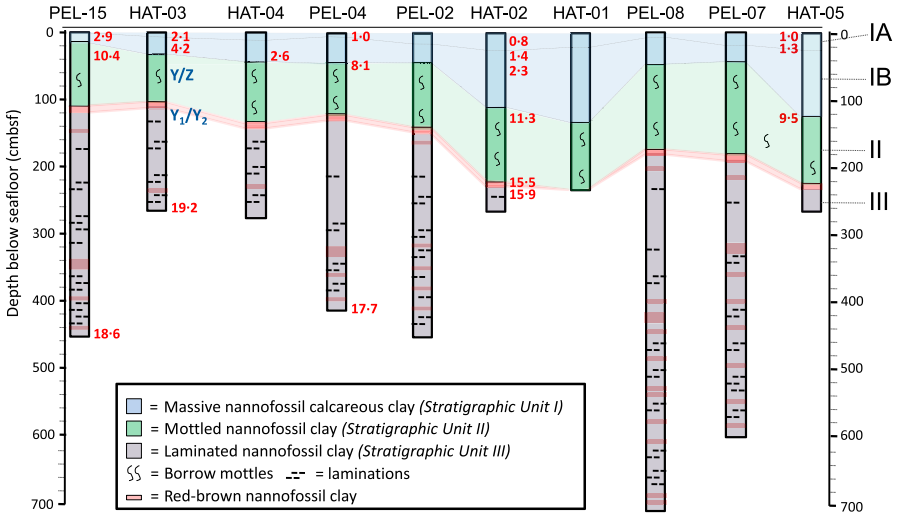

Fig. 2. Stratigraphic correlation of marine sediments over the MC118 site. Cores are arranged by increasing distance (left to right) away from the field. Dates obtained via AMS radiocarbon analysis of planktonic foraminifera (red, Ka) and foraminiferal biostratigraphic boundaries (dark blue, Y/Z *ca* 10 Ka and Y1/Y2 *ca* 15 Ka) are shown alongside their stratigraphic position; all reported ages are in calibrated calendar years BP. Three stratigraphic units are identified as follows: Unit I (light blue) = massive nannofossil calcareous silty clay; Unit II (light green) = mottled nannofossil clay; Unit III (grey) = laminated nannofossil clay containing reddish-brown nannofossil clay layers (red lines); for detailed stratigraphic description see Ingram *et al.* (2010). The distinct *ca* 5-cm thick reddish clay layer ('red band') contains highly 'reworked' (pre-Quaternary) nannofossils and defines the top of Unit III.

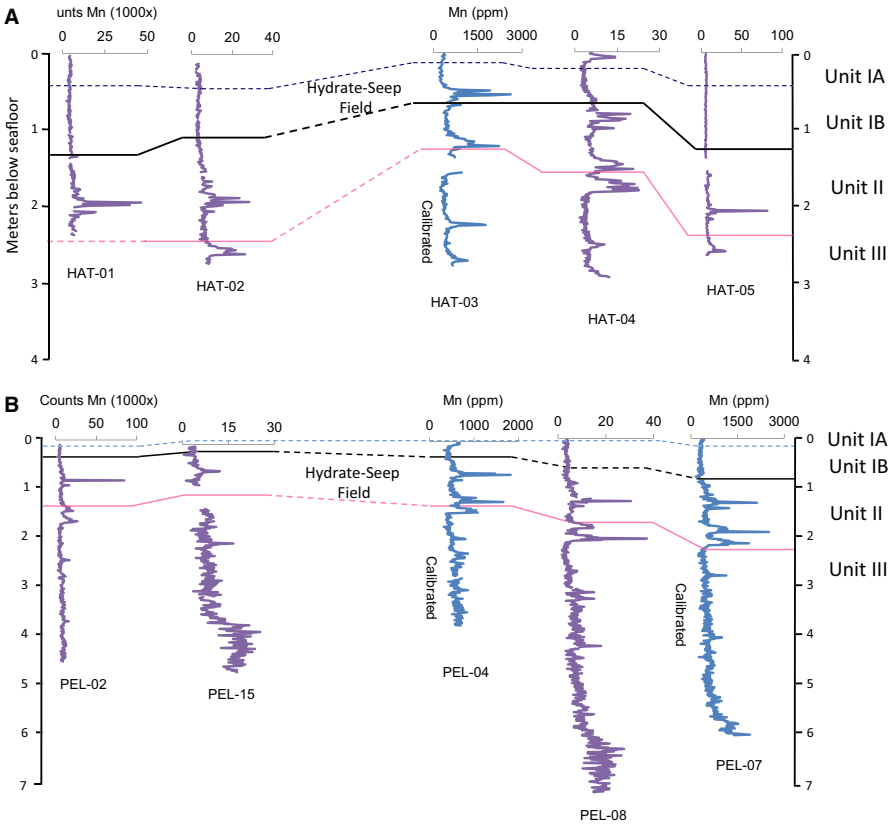

Fig. 3. Profiles of down-core Mn concentration/XRF counts across Transect 1 from the *R/V Hatteras* cruise (A) and across Transect 2 from the *R/V Pelican* cruise (B). Transect 1 is the N-S transect from HAT-01 to HAT-05 displayed in Fig. 1. Transect 2 is the NW-SE transect from PEL-02 to PEL-07 also shown in Fig. 1. Cores HAT-03, PEL-04 and PEL-07 are calibrated to Mn measured by ICP-AES, see Table 1 for calibration of XRF counts to ICP-AES Mn concentration; all other cores are presented here as XRF counts. Down-core profiles display Mn counts (1000x) with lines drawn across the profiles representing stratigraphic boundaries. The black lines separate Unit I from Unit II, which mark a substantial shift in carbonate content. The thin-dashed blue line separates informal units IA and IB, defined by a change in carbonate content (Ingram *et al.*, 2010, 2013). The light-red line is the depth to the 'red band', a chronostratigraphic marker (Ingram *et al.*, 2010), which defines the top of Unit III.

also observed by previous investigators (Lutken *et al.*, 2006; Brunner, 2007; Sleeper & Lutken, 2008; Ingram *et al.*, 2010). This marker bed is coincident with reworked pre-Quaternary nannofossils deposited during Melt Water Pulse 1A (MWP-1A; Marchitto & Wei, 1995), and is dated between 14 000 and 15 000 calendar years BP (Ingram *et al.*, 2010). The unit lacks a defined base, and thus extends to the greatest depth recovered. Based on accumulation rates and radiocarbon dating (Ingram *et al.*, 2010), sediments are latest Pleistocene in age and certainly older than the MWP-1A reworked nannofossil horizon, which defines the top of the unit (Fig. 2).

Manganese profiles spanning units II and III may appear correlative, such as in Cores PEL-04, -08 and -07, yet upon close examination, Mn layers are not chronostratigraphically equivalent (PEL-04, PEL-07 and -08; Fig. 3). It is also apparent that Unit III mostly lacks the highly concentrated Mn-layers, with one exception in Core PEL-08 (near the top of the unit; Fig. 3), yet recovery of this unit was incomplete using shallow gravity coring. The Pelican transect recovered more of Unit III than the previous cruise and yields several metres of late Pleistocene-aged sediments in some cores. While this unit lacks the discrete highly concentrated Mn-layers, it does display many 'minor' layers (Fig. 3).

Mn-layer mineralogy

A multi-step reductive dissolution and acid digestion procedure was used to operationally determine probable mineral phases associated with the authigenic Mn (Fig. 4; Table 2). From five sediment samples taken within the Mn-layers, just over 80 percentage of the total Mn content is comprised of Mn-rich calcite ($Ca\text{-}Mn(CO_3)_2$) and/or rhodochrosite ($MnCO_3$) (Table 2). Manganese oxides account for slightly less than 10 percent, and the 'insoluble' clay fraction accounts for *ca* 10% (Table 2). Thus,

Mn within the concentrated layers is predominantly associated with carbonates, followed by aluminosilicates and minor amounts of oxides. Some change in concentration may be an artefact of the total change in sample mass associated with dissolution of carbonates. This is a concern for sediments with very high carbonate content, however, the samples investigated here (selected for sequential dissolution in PEL-07) are from clay-rich Units II and III with less than 13 wt.% $CaCO_3$ on average. To more rigorously address this issue, Mn enrichment factors and 'excess' Mn are also calculated (Table 2). Manganese enrichment and 'excess' Mn (defined as the non-clay fraction) are largely associated with carbonates and not oxides (Table 2). This is shown by determining the percentage of 'excess' Mn in each respective fraction (oxide verses carbonate) where the clay fraction has already been removed (via calculation of 'excess' Mn). The following expression:

$$((\text{untreated}_{\text{excess}} - \text{carbonate}_{\text{excess}}/\text{untreated}_{\text{excess}})*100)$$

yields only 6·8% of Mn as potentially associated with oxides or oxyhydroxides, based on the average of all five layers (Table 2). Hence, 'excess' Mn from within the Mn-layers is dominantly associated with carbonates (over 90% on average).

Six untreated samples were also analysed using XRD (PEL-07-layer1, PEL-07-layer2, PEL-07-layer3, PEL-07-layer4, PEL-07-layer5 and PEL-04 at 5 cm depth; Fig. 5). All six XRD diffraction results show the existence of the following phases but in different proportions: quartz, calcite, feldspar, dolomite, rhodochrosite and clay minerals. Manganese is present as carbonate or Mn-Fe carbonate, which may form a complete solid solution (Fig. 5). Manganese carbonate in most samples has a d_{104} peak at *ca* 2·82 Å, except sample PEL-07-layer 4 that has a value of 2·827 Å. The d_{104} peak for the pure Mn end member (rhodochrosite) is 2·84 Å, and that for the pure Fe end member (siderite) is 2·79 Å. The d_{104} of the samples indicates a Mn-rich (>50% Mn) carbonate. One acid treated sample taken from PEL-07 (Mn-layer3; Fig. 5B) yielded no carbonates in the diffraction pattern; this result indicates that the dissolution procedure used here and by Chun *et al.* (2010) effectively removes Mn-carbonate minerals.

To summarize, the X-Ray diffraction and reductive dissolution/acidification results reveal that Mn within the

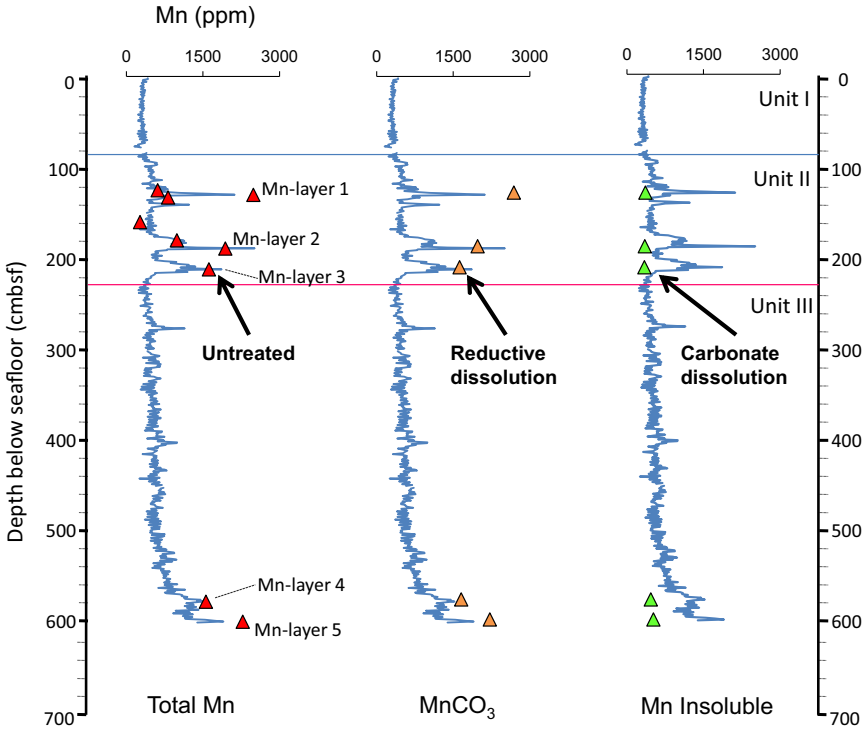

Fig. 4. Calibrated XRF-Mn profile (blue curve) for Core PEL-07 and Mn concentrations (triangles, same scale) following dissolution procedures to operationally determine the likely mineral phases associated with the Mn-layers. From left to right, the red triangles are from untreated sediment samples, orange triangles indicate samples following the reductive dissolution step, and the green triangles represent insoluble (clay) residue following both dissolution procedures. Reductive dissolution removes oxides; hence the remaining concentration comprises carbonate minerals plus insoluble (clay) residue. The following acid-dissolution step removes carbonates, thus only insoluble (clay) residue remains after both steps.

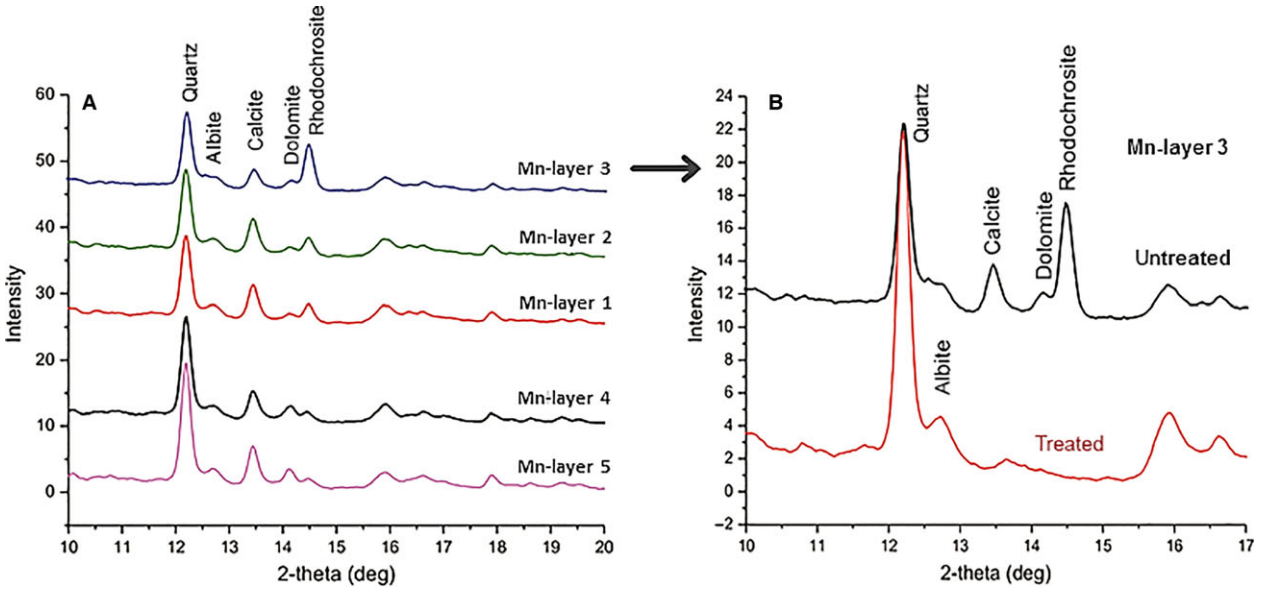

Fig. 5. (A) X-ray diffraction spectra for the five selected Mn-layers in Core PEL-07 (for locations see the numbers on Fig. 4). The mineral diffraction peaks labelled from left to right are quartz, albite, calcite, dolomite and rhodochrosite. The rhodochrosite diffraction peak is present in all samples (Mn-layers), and is largest (most concentrated) in Mn-layer 3. (B) X-ray diffraction spectra for Mn-layer 3, before acid dissolution (black curve), and after acid dissolution (red curve). The other diffraction peaks appear larger, as the carbonate fraction was removed by the acid dissolution, thereby concentrating siliciclastic minerals in the treated sample.

Mn-layers is largely contained in the carbonate phase. Given sample heterogeneity, preferred orientation and different proportions of mineral phases, intensities of the rhodochrosite d_{104} peak is not expected to exactly correlate with the XRF/ICP-AES derived Mn concentration – for example, Mn-layer3 is not the most concentrated based on the XRF profile (Figs 4 and 5). However, Mn-layers 1, 2 and 3 exhibit larger rhodochrosite peaks than Mn-layers 4 and 5 (Fig. 5), which is generally consistent with Mn concentrations from XRF and ICP-AES (Fig. 4; Table 2).

INTERPRETATION AND DISCUSSION

Manganese carbonate layers at MC118

A detailed deep-sea sedimentary record is documented at MC118 in an effort to better understand accumulation of highly enriched Mn-layers and possible mechanisms for their formation. Foremost, it is clear that Mn-layers occur in sediments of different age and generally do not follow lithostratigraphic or chronostratigraphic trends. Hence, their characterization as authigenic deposits, which formed *in situ* through redox processes (Figs 2 and 3), representing diagenetic palaeo-redox horizons. Multi-step chemical dissolution procedures combined with XRD analyses confirms that the Mn-layers are primarily carbonates.

The documentation of such a highly detailed spatio-temporal record of recurring authigenic Mn carbonate layers as observed at MC118 is somewhat unique considering water depth and proximity to the seabed with nearby cold seeps (Canfield *et al.*, 1993; Chun *et al.*, 2010). However, Mn enrichments are often observed in ancient marine sediments or mudstones, along with other elements associated with authigenic deposits, and have been linked to changes in past climate or oceanographic conditions (Dickens & Owen, 1994; Schenau *et al.*, 2002; Tribovillard *et al.*, 2006). The MC118 results indicate that substantial variability in Mn enrichment is present in Recent (Late Pleistocene-Holocene) deep-sea sediments over a relatively small area of the sea floor (*ca* 2 km^2: Fig. 1). This has important implications for interpreting chemostratigraphic records from similar deep-sea depositional environments, as it implies that modern and ancient sedimentary Mn records may reflect localized conditions from depositional heterogeneity, rather than more widespread regional or 'global' events. Thus, subtle variation in depositional or redox environments in deep-marine continental slope sediments may drive noticeable differences in the accumulation of authigenic minerals. The MC118 record shows that authigenic Mn can vary considerably within continental slope sediments over a small area of the sea floor, and suggest linkages to the local gas-hydrate and cold-seep field. This includes sea

floor warping, which is well-documented in salt-dominated margins (Jackson, 1995).

Biogeochemistry of the Mn-carbonate layers

Nearly all of the Mn-layers occur at depths well below expected oxygenated pore waters for this depositional setting, consistent with a Mn-carbonate phase preserved in post-oxic sediments. Previous studies have demonstrated that oxygen depletion occurs within 5 cm of the sea floor for similar settings such as the western Gulf of Mexico Shelf (Hu *et al.*, 2011) and the Mississippi Canyon region (Diaz & Trefry, 2006). More recent studies have reported Mn-enrichments (oxides) within 10 cm of the sea floor at similar water depths and close to the MC118 site (Brooks *et al.*, 2015; Hastings *et al.*, 2016). In contrast, most Mn layers at MC118 are found more than a metre below the sea floor, thus they are considered much too deep for active formation of Mn-oxides, which develop near the oxygen depletion depth (Burdige & Gieskes, 1983; Kalhorn & Emerson, 1984; Heggie *et al.*, 1986; Aller, 1990, 1994; Shaw *et al.*, 1990; Reimers *et al.*, 1992). However, it should also be noted that Mn carbonates can develop a protective crust around oxides formed earlier, thereby diminishing their dissolution within post-oxic pore waters (Burdige, 1993). This protective crust may account for the small fraction (under 10%) of Mn-oxide observed in some layers (Table 2).

Repeated Mn cycling (the 'Mn pump'; Sageman & Lyons, 2003) can concentrate dissolved Mn within alkaline pore waters to form Mn-rich carbonates. Thus, Mn enrichment may form along palaeo-redox boundaries, related to the carbonate-Mn pump, where dissolved Mn concentrated in pore waters leads to precipitation of Mn-carbonate minerals under sufficiently alkaline conditions. Mn-oxide dissolution may occur contemporaneously with formation of Mn-carbonates just beneath an active redox front, followed by subsequent burial and preservation of the palaeo-redox boundary (Pedersen & Price, 1982; Burdige, 2006). The rapid burial of highly concentrated Mn-oxides into deeper dysoxic/anoxic and alkaline pore waters, due to a (pulsed) increase in sedimentation rate, would also promote the preservation of Mn-carbonate layers. More generally, sedimentation can influence redox processes through erosion and/or deposition.

Other factors that drive the movement of the Mn-redox boundary include, but are not limited to, (1) changes in organic carbon delivery and reactivity, (2) bottom water oxygen content, or (3) intensity of bioturbation/bioirrigation. All of the above factors influence preservation of 'relict' Mn-peaks (Burdige, 2006). Most of these factors are not explicitly constrained in this study, although previous efforts quantify sedimentation rates, and organic matter accumulation/composition (Ingram *et al.*, 2013). There is a shift towards more reactive organic matter (Type II) within the shallow Holocene sediments, which is expected to drive the redox boundary upwards, yet this is also balanced by slower sedimentation rates (Ingram *et al.*, 2010). Regardless, there are too many discrete Mn-layers to explain with one stepwise change in sedimentation. Furthermore, while organic matter accumulation is variable with time (Ingram *et al.*, 2013), it should be more uniform spatially in a deep-sea setting – unless it is also influenced by the presence of the seeps. Thus, dynamic sedimentation associated with the mound is hypothesized as a more viable driver to explain spatio-temporal trends of the Mn-peaks across the network of MC118 cores, which suggest the field's influence.

Mapping Mn-carbonate layers: a tool to delineate palaeo-redox conditions

The analysis presented here suggests that the high-resolution Mn record at MC118 primarily reflects the duration of steady-state conditions and the frequency with which they are interrupted, through changes in sedimentation that are driven by local effects from the presence of the elevated bathymetric mound. Relatively more stable sedimentation is expected for core sites farther away from the area of active cold seepage and gas hydrate formation (centred over the bathymetric mound). Such distal sites should be characterized by prolonged periods of steady-state conditions, and hence a more stable palaeo-redox boundary along which more concentrated Mn-layers can form. Conversely, frequent interruption of steady-state conditions is expected in closer proximity to or down-slope from the field yielding less-concentrated and more-numerous Mn-layers (Fig. 2). The distribution of Mn-layers at the site is consistent with this hypothesis, as only one or two very-concentrated authigenic Mn-layers (Cores HAT-01, HAT-05 and PEL-02) are observed at locations distal from the field, while a greater abundance of less-concentrated layers are observed closer to the field (Core HAT-03 and HAT-04, Fig. 3).

Authigenic Mn enrichments are well-documented in marine sediments (Burdige, 1993, 2006), however, it is the remarkable detail of the MC118 record in both time and space that makes this study unique, and reveals past movement of the palaeo-redox boundary at various core sites. This record is made possible through the application of high-resolution XRF scanning techniques. The integration of such spatio-temporal data with quantitative biogeochemical models for Mn-cycling should provide a powerful new tool for evaluating redox cycling and/or sedimentation events over a wide range of time scales, for example, quantification of the duration of steady state

conditions required to generate a Mn-layer of given concentration (Froelich *et al.*, 1979; Burdige & Gieskes, 1983; Finney *et al.*, 1988; Burdige, 1993; Price, 1998), and deconvolution of local versus regional/global influences on the observed Mn record.

CONCLUSIONS

The results presented here demonstrate that multiple discrete Mn-layers observed at MC118 are authigenic deposits, preserved as carbonates and formed within shallow sediments along a transient palaeo-redox boundary. The Mn-layers occur independently from established lithostratigraphic and chronostratigraphic horizons at the site, and results from sequential extraction procedures, along with XRD analysis, reveal that layers are mostly rhodochrosite ($MnCO_3$). It is not known if the Mn-layers formed initially in shallow sediments as oxides/oxyhydroxides or as carbonates, however, they are presently carbonate minerals preserved within post-oxic conditions.

The spatio-temporal heterogeneity of this Mn record is linked to the MC118 gas-hydrate and cold-seep field, including the related salt diapirism beneath the mound. This sea floor feature and associated release of hydrocarbons in turn influenced palaeo-redox cycling and/or sedimentation processes that impacted the duration of steady-state conditions in the past. Thus, the concentrations and frequency of Mn-layers across the site is a fingerprint of the palaeo-redox boundary and its spatial expression with time. While numerous factors drive changes in redox conditions, it is suggested that variability in sedimentation rate, caused by the presence of the sea floor mound, is a viable mechanism to explain the complexity of the Mn record.

ACKNOWLEDGEMENTS

Financial support for this research was provided by university and departmental funds to Dr. Stephen Meyers (UNC-Chapel Hill and UW-Madison). Additional support was provided by the Gulf of Mexico Gas Hydrate Research Consortium (HRC grants 300212198E (UM 07-01-071) and 300212260E (UM 08-11-047) to C.S. Martens), and funding for ship time on the R/V Pelican was provided by Minerals Management Services (now Department of Ocean Energy) and NOAA's National Institute for Undersea Science and Technology. Funding for the R/V Hatteras Cruise, ship time and coring operations was provided by the Duke/UNC Oceanographic Consortium as part of a joint proposal with other UNC investigators, Kai Ziervogel, Drew Steen and Carol Arnosti. The crew, joint investigators listed above, Sherif Ghobrial, Carol Lutken and Ken Sleeper were all instrumental in the shipboard core collection process that provided the material used for this study.

References

Aller, R.C. (1990) Bioturbation and manganese cycling at the sediment-water interface. *Philos. Trans. R. Soc. London*, **331**, 51–68.

Aller, R.C. (1994) The sedimentary cycle in Long Island Sound: its role as intermediate oxidant and the influence of bioturbation, O_2, and C_{org} flux on diagenetic reaction balances. *J. Mar. Resour.*, **52**, 259–295.

Brooks, G.R., Larson, R.A., Schwing, P.T., Romero, I., Moore, C., Reichart, G.-J., Jilbert, T., Chanton, J.P., Hastings, D.W., Overholt, W.A., Marks, K.P., Kostka, J.E., Holmes, C.W. and **Hollander, D.** (2015) Sedimentation pulse in the NE Gulf of Mexico following the 2010 DWH blowout. *PLoS ONE*, **10**, 1–24, e0132341.

Brunner, C.A. (2007) *Stratigraphy and Palaeoenvironment of Shallow Sediments from MC118*. Proceedings of the Annual Meeting of the Gulf of Mexico Hydrate Research Consortium, October 10–11, 2007, Oxford, Mississippi.

Burdige, D.J. (1993) The biogeochemistry of manganese and iron reduction in marine sediments. *Earth Sci. Rev.*, **35**, 249–284.

Burdige, D.J. (2006) *Geochemistry of Marine Sediments*. Princeton University Press, Princeton, NJ, 609 pp.

Burdige, D.J. and **Gieskes, J.M.** (1983) A pore water/solid phase diagenetic model for manganese in marine sediment. *Am. J. Sci.*, **283**, 29–47.

Canfield, D.E., Thamdrup, B. and **Hansen, J.W.** (1993) The anaerobic degradation of organic matter in Danish coastal sediments: Fe reduction, Mn reduction, and sulfate reduction. *Geochim. Cosmochim. Acta*, **57**, 3867–3883.

Castellini, D.G., Dickens, G.D., Snyder, G.T. and **Ruppel, C.D.** (2006) Barium cycling in shallow sediments above active mud volcanoes in the Gulf of Mexico. *Chem. Geol.*, **226**, 1–30.

Chun, C.O.J., Delaney, M.L. and **Zachos, J.C.** (2010) Palaeoredox changes across the Palaeocene-Eocene thermal maximum, Walvis Ridge (ODP Sites 1262, 1263, and 1266): evidence from Mn and U enrichment factors. *Paleoceanography*, **25**, 1–13.

Diaz, R.J. and **Trefry, J.H.** (2006) Comparison of sediment profile image data with profiles of oxygen and Eh from sediment cores. *J. Mar. Syst.*, **62**, 164–172.

Dickens, G.R. (2001) The potential volume of oceanic methane hydrates with variable external conditions. *Org. Geochem.*, **32**, 1179–1193.

Dickens, G.R. (2003) Rethinking the global carbon cycle with a large dynamic and microbially mediated gas hydrate capacitor. *Earth Planet. Sci. Lett.*, **213**, 169–183.

Dickens, G.R. and **Owen, R.M.** (1994) Late Miocene-Early Pliocene manganese redirection in the central Indian Ocean:

expansion of the intermediate water oxygen minimum zone. *Paleoceanography*, **9**, 169–181. doi:10.1029/93PA02699.

Dickens, G.R., O'Neil, J.R., Rea, D.K. and **Owen, R.M.** (1995) Dissociation of oceanic methane hydrate as a cause of the carbon isotope excursion at the end of the Palaeocene. *Paleoceanography*, **10**, 965–971.

Diegel, F.A., Karlo, J.F., Schuster, D.C., Shoup, R.C. and **Tauvers, R.C.** (1995) Cenozoic structural evolution and tectono-stratigraphic framework of the northern Gulf Coast continental margin. In: *Salt Tectonics: A Global Perspective* (Eds M.P.A. Jackson, D.G. Roberts and S. Snelson), *Am. Assoc. Petrol. Geol. Mem.*, **65**, 109–151.

Feng, D., Birgel, D., Peckmann, J., Roberts, H.H., Joye, S.B., Sassen, R., Liu, X.-L., Hinricks, K.-U. and **Chen, D.** (2014) Time integrated variation of sources of fluids and seepage dynamics archived in authigenic carbonates from Gulf of Mexico Gas Hydrate Seafloor Observatory. *Chem. Geol.*, **385**, 129–139.

Finney, B.P., Lyle, M.W. and **Heath, G.R.** (1988) Sedimentation at MANOP site H (eastern Equatorial Pacific) over the past 400,000 years: climatically induced redox variations and their effects on transient metal cycling. *Paleoceanography*, **3**, 169–189.

Froelich, P.N., Klinkhammer, G.P., Bender, M.L., Luedtke, N., Heath, G.R., Cullen, D., Dauphin, P., Hammond, D., Hrtman, B. and **Maynard, V.** (1979) Early oxidation of organic matter in pelagic sediments of the eastern equatorial Atlantic: suboxic diagenesis. *Geochim. Cosmochim. Acta*, **43**, 1075–1090.

Galloway, W.E., Ganey-Curry, P.E., Li, X. and **Buffler, R.T.** (2000) Cenozoic depositional history of the Gulf of Mexico basin. *Am. Assoc. Petrol. Geol. Bull.*, **84**, 1743–1774.

Ginsburg, G.D. (1998) Gas hydrate accumulation in deep-water marine sediments. In: *Gas Hydrates: Relevance to World Margin Stability and Climate Change* (Eds J.P. Henriet and J. Mienert), *Geol. Soc. London. Spec. Publ.*, **137**, 51–62.

Haq, B.U. (1998) Natural gas hydrates: searching for the long-term climatic and slope-stability records. In: *Gas Hydrates: Relevance to World Margin Stability and Climate Change* (Eds J.P. Henriet and J. Mienert), *Geol. Soc. London. Spec. Publ.*, **137**, 303–318.

Hastings, D.W., Schwing, P.T., Brooks, G.R., Larson, R.A., Morford, J.L., Roeder, T., Quinn, K.A., Bartlett, T., Romero, I.C. and **Hollander, D.J.** (2016) Changes in sediment redox conditions following the BP DWH blowout event. *Deep-Sea Res. II*, **129**, 167–178.

Heggie, D.T., Kahn, D. and **Fischer, K.** (1986) Trace metals in metalliferous sediments, MANOP site M: interfacial pore water profiles. *Earth Planet. Sci. Lett.*, **80**, 106–116.

Hu, X., Cai, W.J., Wang, Y., Guo, X. and **Lou, S.** (2011) Geochemical environments of continental shelf-upper slope sediments in the northern Gulf of Mexico. *Palaeogeogr. Palaeoclimatol. Palaeoecol.*, **312**, 265–277.

Ingram, W.C., Meyers, S.R., Brunner, C.B. and **Martens, C.S.** (2010) Late Pleistocene-Holocene sedimentation surrounding an active seafloor gas-hydrate and cold-seep field on the Northern Gulf of Mexico Slope. *Mar. Geol.*, **278**, 43–53.

Ingram, W.C., Meyers, S.R. and **Martens, C.S.** (2013) Controls on sedimentary Geochemistry and organic carbon burial at a large gas-hydrate and cold-seep field on the northern Gulf of Mexico Slope. *Mar. Pet. Geol.*, **46**, 190–200.

Jackson, M.P.A. (1995) Retrospective Salt Tectonics. In: *Salt Tectonics: A Global Perspective* (Eds M.P.A. Jackson, D.G. Roberts and S. Snelson), *Am. Assoc. Petrol. Geol. Mem.*, **65**, 1–28.

Kalhorn, S. and **Emerson, S.** (1984) The oxidation state of manganese in surface sediments of the deep sea. *Geochem. Cosmochim. Acta*, **48**, 897–902.

Kvenvolden, K.A. (1988) Methane Hydrate – a major reservoir of carbon in the shallow geosphere? *Chem. Geol.*, **71**, 41–51.

Lapham, L.L., Chanton, J.P., Martens, C.S., Sleeper, K. and **Woolsey, J.R.** (2008) Microbial activity in surficial sediments overlying acoustic wipeout zones at a Gulf of Mexico cold seep. *Geochem. Geophys. Geosyst.*, **9**, 1–17.

Lapham, L.L., Chanton, J.P., Chapman, R. and **Martens, C.S.** (2010) Methane under-saturated fluids in deep-sea sediments: implications for gas hydrate stability and rates of dissolution. *Earth Planet. Sci. Lett.*, **298**, 275–285. doi:10.1016/j.epsl.2010.07.016.

Lutken, C.B., Brunner, C.A., Lapham, L.L., Chanton, J.P., Rogers, R., Sassen, R., Dearman, J., Lynch, L., Kuykendall, J. and **Lowrie, A.** (2006) *Analyses of Core Samples from the Mississippi Canyon 118, Paper OTC 18208*. Offshore Technology Conference, American Association of Petroleum Geologist, May 1–4, 2006, Houston, TX.

Macelloni, L., Simonetti, A., Knapp, J.H., Knap, C.C., Lutken, C.B. and **Lapham, L.L.** (2012) Multiple resolution seismic imaging of a shallow hydrocarbon plumbing system, Woolsey Mound, Northern Gulf of Mexico. *Mar. Pet. Geol.*, **38**, 128–142.

Macelloni, L., Brunner, C.A., Caruso, S., Lutken, C.B., D'Emidio, M. and **Lapham, L.L.** (2013) Spatial distribution of seafloor bio-geological and geochemical proxies of fluid regime and evolution of a carbonate/hydrates mound, northern Gulf of Mexico. *Deep Sea Res. Part I*, **74**, 25–38.

Marchitto, T.M. and **Wei, K.Y.** (1995) History of the Laurentide meltwater flow to the Gulf of Mexico during the last deglaciation, as revealed by reworked calcareous nannofossils. *Geology*, **23**, 779–782.

Martens, C.S., Medlovitz, H.P., Seim, H., Lapham, L. and **D'Emidio, M.** (2016) Sustained in situ measurements of dissolved oxygen, methane and water transport processes in the benthic boundary layer at MC118 northern Gulf of Mexico. *Deep-Sea Res. II*, **129**, 41–52.

Maslin, M., Mikkelsen, N., Vilela, C. and **Haq, B.** (1998) Sea-level and gas-hydrate-controlled catastrophic sediment failures of the Amazon Fan. *Geology*, **26**, 1107–1110.

Maslin, M., Owen, M., Day, S. and **Long, D.** (2004) Linking continental-slope failures and climate change: testing the clathrate gun hypothesis. *Geology*, **32**, 53–56.

McGee, T. (2006) A seafloor observatory to monitor gas hydrates in the Gulf of Mexico. *Lead. Edge*, **25**, 644–647.

McGee, T., Lutken, C., Rogers, R., Brunner, C., Dearman, J., Lynch, F. and **Woolsey, R.** (2009) Can fractures in soft sediments host significant quantities of gas hydrates? *Geol. Soc. London. Spec. Publ.*, **319**, 29–49.

Mienert, J., Vanneste, M., Bunz, S., Andreassen, K., Haflidson, H. and **Sejrup, H.P.** (2005) Ocean warming and gas hydrate stability on the mid-Norwegian Margin at the Storegga Slide. *Mar. Pet. Geol.*, **22**, 233–244.

Milkov, A.V. (2004) Global estimates of hydrate-bound gas in marine sediments: how much is really out there? *Earth Sci. Rev.*, **66**, 183–197.

Nisbet, E.G. (1990) The end of the ice-age. *Can. J. Earth Sci.*, **27**, 148–157.

Paull, C.K., Buelow, W.J., Ussler, W., III and **Borowski, W.S.** (1996) Increased continental-margin slumping frequency during sea-level lowstands above gas-hydrate-bearing sediments. *Geology*, **24**, 143–146.

Paull, C.K., Brewer, P.G., Ussler, W., III, Peltzer, E.T., Rehder, G. and **Clague, D.** (2003) An experiment demonstrating that marine slumping is a mechanism to transfer methane from gas-hydrate deposits into the upper ocean and atmosphere. *Geo-Mar. Lett.*, **22**, 198–203.

Paull, C.K., Ussler, W., Lorenson, T.D., Winters, W. and **Dougherty, J.A.** (2005) Geochemical constraints on the distribution of gas hydrates in the Gulf of Mexico. *Geo-Mar. Lett.*, **25**, 273–280.

Pedersen, T.F. and **Price, N.B.** (1982) The geochemistry of manganese carbonate in Panama Basin sediments. *Geochim. Cosmochim. Acta*, **46**, 59–68.

Price, B.A. (1998) *Equatorial Pacific Sediments: A Chemical Approach to Ocean History*. PhD Diss. Scripps Institute of Oceanography, UCSD, San Diego, CA, 364 pp.

Reimers, C.E., Jahnke, R.A. and **McCorkle, D.C.** (1992) Carbon fluxes and burial rates over the continental slope and rise off central California with implications for the global carbon cycle. *Global Biogeochem. Cycles*, **6**, 199–224.

Richter, T.O., Van Der Gaast, S., Koster, B., Vaars, A., Gieles, R., De Stigter, H.C., De Haas, H. and **Van Weering, T.C.E.** (2006) The Avaatech XRF Core Scanner: technical description and applications to NE Atlantic sediments. In: *New ways of Looking at Sediment Core and Core Data* (Ed. R.G. Rothwell), pp. 39–50. Geological Society Special Publication, London.

Rudnick, R.L. and **Gao, S.** (2003) Composition of the continental crust. In: *Treatise on Geochemistry* (Eds D.H. Heinrich and K.T. Karl), pp. 1–64. Pergamon, Oxford, UK.

Sageman, B.B. and **Lyons, T.W.** (2003) Geochemistry of fine-grained sediments and sedimentary rocks. In: *Treatise on Geochemistry*, Vol. 7 (Ed. F. MacKenzie), pp. 115–158. Elsevier, New York, NY.

Sassen, R., Roberts, H.H., Carney, R., Milkov, A.V., DeFreitas, D.A., Lanoil, B. and **Zhang, C.L.** (2004) Free hydrocarbon gas, gas hydrate, and authigenic minerals in chemosynthetic communities of the northern Gulf of Mexico continental slope: relation to microbial processes. *Chem. Geol.*, **205**, 195–217.

Sassen, R., Roberts, H.H., Jung, W., Lutken, C.B., DeFreitas, D.A., Sweet, S.T. and **Guinasso, N.L. Jr** (2006) *The Mississippi Canyon 118 Gas Hydrate Site: A Complex Natural System Paper OTC 18132*. Offshore Technology Conference, May 1–4, Houston, TX.

Schenau, S.J., Reichart, G.J. and **De Lange, G.J.** (2002) Oxygen minimum zone controlled Mn redistribution in Arabian Sea sediments during the late Quaternary. *Paleoceanography*, **17**, 1058. doi:10.1029/2000PA000621.

Shaw, T.J., Gieskes, J.M. and **Jahnke, R.A.** (1990) Early diagenesis in differing depositional environments: the response of transitional metals in pore water. *Geochem. Cosmochim. Acta*, **54**, 1233–1246.

Simonetti, A., Knapp, J.H., Sleeper, K., Lutken, C.B., Macelloni, L. and **Knapp, C.C.** (2013) Spatial distribution of gas hydrates from high-resolution seismic and core data, Woolsey Mound, Northern Gulf of Mexico. *Mar. Pet. Geol.*, **44**, 21–33.

Sleeper, K.A. and **Lutken, C.** (2008) *Activities Report for Cruise GOM1-08-MC118 Aboard the R/V Pelican Sampling and Deployment Cruise Mississippi Canyon Federal Lease Block 118 Northern Gulf of Mexico April 22–28, 2008*. The Center for Marine Resources and Environmental Technology and the Seabed Technology Research Center, University of Mississippi. Available at: http://www.olemiss.edu/depts/mmri/programs/ppt_list.html.

Sleeper, K.A., Lowrie, A., Bosman, A., Macelloni, L. and **Swann, C.T.** (2006) *Bathymetric Mapping and High Resolution Seismic Profiling by AUV in MC 118 (Gulf of Mexico)*. Paper OTC 18133, Offshore Technology Conference, Houston, TX.

Tribovillard, N., Algeo, T.J., Lyons, T. and **Armelle, R.** (2006) Trace metals as palaeoredox and palaeoproductivity proxies: an update. *Chem. Geol.*, **232**, 12–32.

